

I.

VECTOR MESON  
DOMINANCE AND POINTLIKE  
COUPLING OF THE PHOTON



# VECTOR MESON DOMINANCE\*

## - selected topics -

G. Piller and W. Weise

Institute of Theoretical Physics  
University of Regensburg  
D - 8400 Regensburg, W. Germany

**Abstract:** We summarize and discuss phenomena related to the vector meson dominance (VMD) of electromagnetic hadron currents. This includes VMD implications for pion and nucleon electromagnetic form factors and shadowing effects seen in the interactions of real and virtual high energy photons with nuclei. In particular, we discuss deep inelastic lepton-nucleus scattering at small values of the Bjorken variable  $x = Q^2/2M\nu$ .

## 1. INTRODUCTION: ELECTROMAGNETIC CURRENTS OF HADRONS

Hadrons interact with photons through the electromagnetic currents of their quark constituents. The fundamental electromagnetic current is

$$J_\mu(x) = \bar{q}(x)\gamma_\mu Q q(x) \quad (1)$$

where  $q(x)$  are the quark fields. For  $N_f = 3$  flavours,

$$q = \begin{pmatrix} u \\ d \\ s \end{pmatrix}, \quad (2)$$

and  $Q$  is the quark electric charge,

$$Q = \frac{1}{2}(B + S + \tau_3) \quad (3)$$

which involves the baryon number  $B = 1/3$ , strangeness  $S$  ( $= -1$  for the s-quark, 0 for u,d-quarks) and isospin  $\tau_3$  ( $\pm 1$  for u,d-quarks, 0 for the s-quark). At high energies and

---

\*Work supported in part by BMFT grant 06 OR 762

momentum transfers in the multi-GeV range, QCD is perturbative and the elementary current quarks are directly visible. At low energies, where hadrons (rather than quarks) are the relevant degrees of freedom, the currents (1) are realized in the form of vector mesons ( $\rho, \omega, \phi, \dots$ ). This is the basic idea behind the Vector Meson Dominance (VMD) model.

## 2. ELECTRON- POSITRON ANNIHILATION INTO HADRONS

Consider current matrix elements  $\langle 0 | J_\mu | \text{hadrons} \rangle$ , which describe the formation of hadronic states out of the vacuum through electromagnetic interactions. These matrix elements are measured in the process  $e^+e^- \rightarrow \text{hadrons}$ . The data are shown in Figs. 1, 2. At  $e^+e^-$  center-of-mass energies  $\sqrt{s} < 1 \text{ GeV}$ , the  $e^+e^- \rightarrow \text{hadron}$  spectrum is visibly dominated by the  $\rho(770)$ ,  $\omega(783)$  and  $\phi(1020)$ . The region  $\sqrt{s} > 1 \text{ GeV}$  extends into the domain of heavy quarks with a continuum plateau and heavy vector mesons of the  $J/\Psi$  and  $\Upsilon$  families. The fact that the  $\rho, \omega$  and  $\phi$  completely dominate the low energy electromagnetic excitation spectrum suggests the current field identity [1]

$$J_\mu^{e.m.}(x) = \sum_{V=\rho^0, \omega, \phi} \frac{m_V^2}{f_V} V_\mu(x), \quad (4)$$

where  $V_\mu = \rho_\mu^0$ ,  $\omega_\mu$  and  $\phi_\mu$  are the respective vector meson fields,  $m_V$  are their masses and  $f_V$  their decay constants (empirically,  $f_\rho \simeq 5.3$ ,  $f_\omega \simeq 15.2$  and  $f_\phi \simeq 13.4$ ). The current-field identity (4) is the basis of a remarkably successful phenomenology. For example, the accuracy of the model in predicting various radiative decay widths of mesons is generally at the 10 % level (see ref. [2] for a recent survey). We continue here by summarizing briefly the role which VMD plays in hadron electromagnetic form factors at  $|q^2| \leq 1 \text{ GeV}^2$ .

## 3. VMD PHENOMENOLOGY AT WORK: PION FORM FACTOR

A well-known demonstration of the degree to which VMD works is the pion form factor  $F_\pi(q^2)$ . It is measured to high accuracy in the spacelike region  $q^2 < 0$  by pion-electron scattering experiments [3] and in the timelike region  $q^2 > 0$  by  $e^+e^- \rightarrow \pi^+\pi^-$ . The data are shown in Fig. 3. The timelike region exhibits the strong dominance of the  $\rho^0$  resonance.

The pion form factor can be written as a dispersion relation,

$$F_\pi(q^2) = 1 + \frac{q^2}{\pi} \int_{4m_\pi^2}^\infty dt \frac{\text{Im } F_\pi(t)}{t(t - q^2 + i\epsilon)}. \quad (5)$$

Here the imaginary part  $\text{Im } F_\pi(t)$  represents the  $\pi^+\pi^-$  mass spectrum with its strong

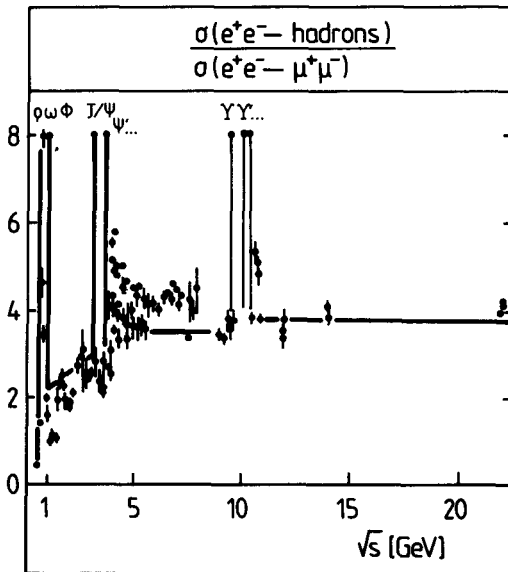


**Figure 1:** Ratio of the total cross section for the  $e^+e^-$  amplitude into hadrons to the muon pair production cross section  $\sigma(e^+e^- \rightarrow \mu^+\mu^-) = \frac{4\pi\alpha^2}{3s}$ .

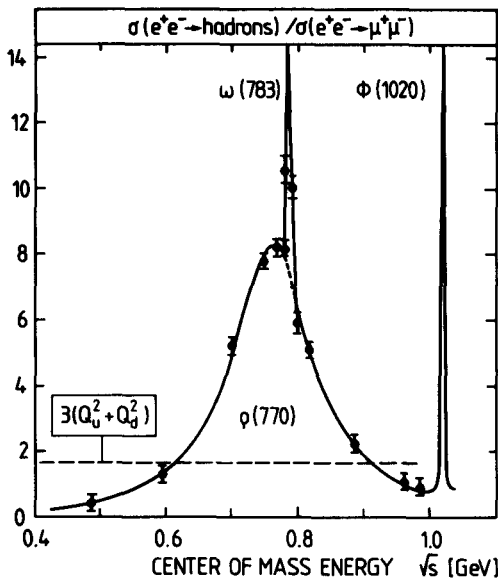


**Figure 2:** Low energy part of the ratio  $\sigma(e^+e^- \rightarrow \text{hadrons})/\sigma(e^+e^- \rightarrow \mu^+\mu^-)$ , showing the dominance of vector mesons ( $\rho, \omega, \phi$ ).

resonant peak at  $t = m_\rho^2 \simeq 0.6 \text{ GeV}^2$ . The electromagnetic pion radius is given by

$$\langle r_\pi^2 \rangle = \left( \frac{6dF_\pi}{dq^2} \right)_{q^2=0} = \frac{6}{\pi} \int_{4m_\pi^2}^\infty \frac{dt}{t^2} \text{Im } F_\pi(t). \quad (6)$$

Hence the pion size as seen by a photon is determined by the low mass part of the  $J^\pi = 1^-$ , isospin  $I = 1$  mesonic spectrum. The VMD assumption is that this spectrum is dominated by the  $\rho$  meson. The current-field identity (4) restricted to the  $\rho$  meson implies  $\text{Im } F_\pi(t) = \pi m_\rho^2 \delta(t - m_\rho^2)$ , and one finds

$$\langle r_\pi^2 \rangle^{1/2} = \frac{\sqrt{6}}{m_\rho} \simeq 0.63 \text{ fm}, \quad (7)$$

which is remarkably close to the measured radius  $\langle r_\pi^2 \rangle^{1/2} = (0.66 \pm 0.01) \text{ fm}$  [4]. Corrections to the naive VMD model, mainly related to a realistic description of the  $2\pi$  continuum have been discussed in the literature and must of course be taken into account in a more detailed quantitative analysis.

#### 4. HADRONIC STRUCTURE OF THE PHOTON

Consider a photon of energy  $\nu$  and momentum  $\vec{q}$ , i.e. with squared four-momentum  $q^2 = \nu^2 - \vec{q}^2 = -Q^2$ . Its propagator, including vacuum polarization effects, can be written in terms of a spectral representation:

$$D_{\mu\nu}(q^2) = -g_{\mu\nu} \left[ \frac{Z}{q^2 + i\epsilon} - \int_{\mu_0^2}^\infty \frac{d\mu^2}{\mu^2} \frac{\Pi(\mu^2)}{q^2 - \mu^2 + i\epsilon} \right] + (q_\mu q_\nu - \text{terms}). \quad (8)$$

The polarization function  $\Pi(\mu^2)$  describes the mass spectrum of intermediate states that contribute to vacuum polarization. In the following, we consider only hadronic vacuum polarization, the process shown in Fig. 4 by which a photon creates virtual quark-antiquark pairs which evolve into hadrons. The lightest hadronic system that can be formed in this way is  $\pi^+ \pi^-$ . Hence the threshold in the integral in eq. (8) is  $\mu_0^2 = 4m_\pi^2$ . The Z factor gives the reduced probability of finding the photon in a "bare" state, and the  $q_\mu q_\nu$  terms guarantee gauge invariance.

The spectral function  $\Pi(\mu^2)$  is a measured quantity. Consider the process  $e^+ e^- \rightarrow \text{hadrons} \rightarrow e^+ e^-$  at a c.m. energy  $\sqrt{s}$ . Its amplitude is proportional to the hadronic polarization part of the photon propagator  $D_{\mu\nu}(s)$ . The cross section  $\sigma(e^+ e^- \rightarrow \text{hadrons})$  is then proportional to the imaginary part of this amplitude, and hence to  $\Pi(s)$ .

One finds

$$\begin{aligned} \Pi(s) &= \frac{s}{\pi e^2} \sigma(e^+ e^- \rightarrow \text{hadrons}) \\ &= \frac{1}{12\pi^2} \frac{\sigma(e^+ e^- \rightarrow \text{hadrons})}{\sigma(e^+ e^- \rightarrow \mu^+ \mu^-)}, \end{aligned} \quad (9)$$

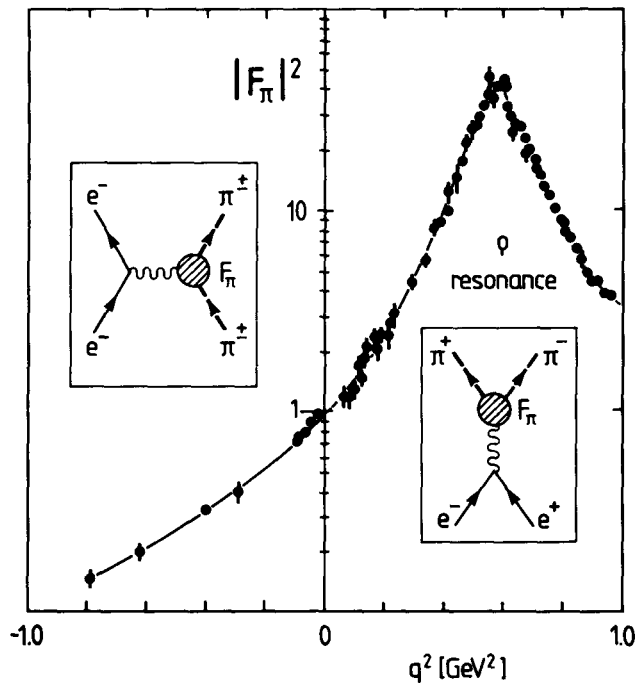


Figure 3: Pion Formfactor; Data from ref. [3].

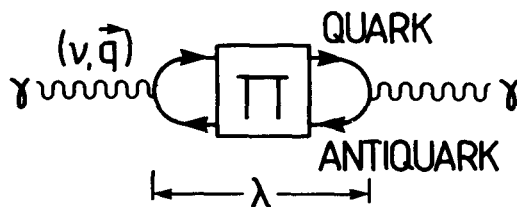


Figure 4: Hadronic vacuum polarisation process.

where the cross section ratio on the right hand side is just the one shown in Figs. 1,2. We now introduce a length scale which is of crucial importance for our further discussions: the propagation length (or coherence length)  $\lambda$  of a hadronic fluctuation when it appears in the vacuum polarization process, Fig. 4. Let  $\mu$  be the mass of this hadronic intermediate state. Then the lifetime of the fluctuation is  $\hbar/\Delta E$  where  $\Delta E = \sqrt{\vec{q}^2 + \mu^2} - \nu$ , the difference between the energy of the hadronic state and the photon energy. Using  $Q^2 = \vec{q}^2 - \nu^2$  and assuming that the fluctuation travels with a velocity close to the speed of light (i.e.  $\mu \ll \nu$ ), we have

$$\lambda \simeq \frac{2\nu}{Q^2 + \mu^2}. \quad (10)$$

As an example, consider a real photon with  $Q^2 = 0$  and  $\nu = 10$  GeV. Then a  $\rho$  meson intermediate state with  $\mu = m_\rho \sim 4 \text{ fm}^{-1}$  has a coherence length  $\lambda > 6 \text{ fm}$ , comparable to the sizes of heavy nuclei.

For later purposes when discussing virtual photons in deep inelastic scattering, it is useful to rewrite  $\lambda$  in terms of the Bjorken scaling variable  $x = Q^2/2M\nu$  (in the lab. frame), where  $M$  is the nucleon mass:

$$\lambda \simeq \frac{1}{Mx} \left( \frac{Q^2}{Q^2 + \mu^2} \right). \quad (11)$$

For  $Q^2 \gg \mu^2$  we see that  $\lambda \simeq 1/Mx$  starts to reach nuclear length scales when  $x < 0.1$ . One therefore expects that processes such as deep inelastic muon scattering at small  $x$  will be strongly influenced by phenomena related to the sizeable coherence length of photon-like hadronic fluctuations.

## 5. SHADOWING

Consider the Compton scattering of a real or virtual photon from a nucleon or nucleus. We prefer a description in the laboratory frame in which the photon has energy  $\nu$  and squared four-momentum  $Q^2$ . A hadronic component of the photon with mass  $\mu$  then travels over a distance  $\lambda = 2\nu/(Q^2 + \mu^2)$ . If this coherence length becomes comparable to typical nuclear dimensions, then the Compton scattering process will undergo the lab. frame time ordering sketched in Fig. 5: the photon converts into hadrons which then scatter on the target nucleons. Single scattering leads to  $\sigma_{\gamma A} = A\sigma_{\gamma N}$ , i.e. the  $\gamma$ -nuclear cross section is then just an incoherent sum of the cross sections for individual nucleons. For sufficiently large propagation length  $\lambda$ , however, multiple scattering can occur, which leads to  $\sigma_{\gamma A} = A^\alpha \sigma_{\gamma N}$  with  $\alpha < 1$ . This is the so-called shadowing effect.

### 5.1 Shadowing in Total Photon-Nucleus Cross Sections

For real photons, nuclear shadowing is a well established phenomenon at energies  $\nu > 5$  GeV. Note that at these energies, the coherence length of vector mesons is

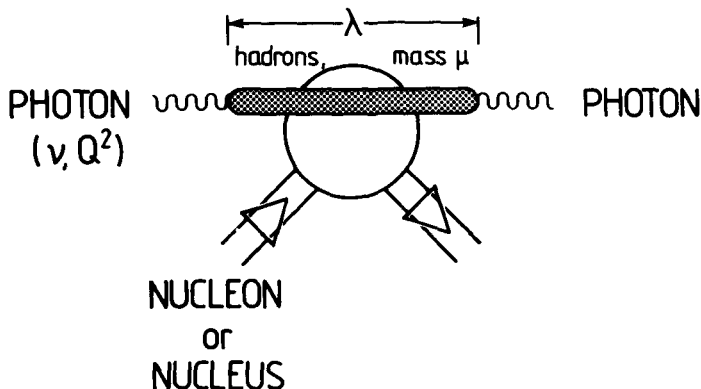


Figure 5: Illustration of high energy Compton scattering on nucleons or nuclei through scattering of hadronic intermediate states.

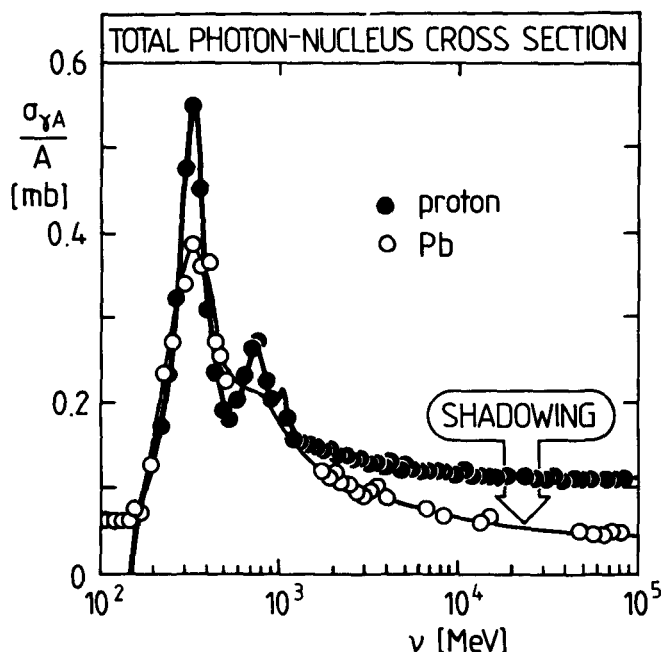


Figure 6: Comparison of the total photon-proton cross section and the photon-nuclear cross section for  $^{208}Pb$ . Data from ref. [4].

$\lambda_{\rho,\omega} \simeq 2\nu/m_{\rho,\omega}^2 > 3 \text{ fm}$ , i.e. it already exceeds the average distance  $d \simeq 2 \text{ fm}$  between nucleons in the center of nuclei. Hence double scattering of vector mesons from nucleons in the nucleus starts to become relevant.

The empirical data above  $\nu > 5 \text{ GeV}$  can be parametrized in the form [5]

$$\sigma_{\gamma A} \simeq A^{0.9} \sigma_{\gamma N}. \quad (12)$$

An example is given for  ${}^{208}\text{Pb}$  in comparison with the free proton in Fig. 6. We observe there that the shadowing starts to develop at photon energies around 2 GeV and stabilizes above 5 GeV.

The VMD interpretation of this effect has been subject of much work in the mid seventies [5, 6]. The basic picture is that of Fig. 5, but now with the hadronic intermediate states dominated by the vector mesons  $V = \rho, \omega, \phi, \dots$ ; the VMD principle then implies

$$\frac{\sigma_{\gamma A}}{\sigma_{\gamma N}} = \frac{\sum_V \sigma_{VA}/f_V^2}{\sum_V \sigma_{VN}/f_V^2} \quad (13)$$

where  $\sigma_{VN}$  and  $\sigma_{VA}$  are the vector meson-nucleon and -nucleus cross sections. One can connect these cross sections by multiple scattering theory and finds (for the example of a Gaussian nuclear density):

$$\sigma_{VA} = A\sigma_{\gamma N} \left[ 1 - \frac{3}{8\pi} \frac{A\sigma_{VN}}{R_A^2} + \dots \right], \quad (14)$$

where  $R_A$  is the nuclear radius. At the same time, the analysis of vector meson photoproduction experiments on the proton [6] leads to  $\sigma_{\rho N} \simeq \sigma_{\omega N} \simeq 25 \text{ mb}$  and  $\sigma_{\phi N}/\sigma_{\rho N} \sim m_\rho^2/m_\phi^2$ . This gives already a rough idea about the effects which generate the "shadow" in eq. (12).

## 5.2 Shadowing in Deep-Inelastic Scattering on Nuclei

Deep inelastic muon scattering on a variety of nuclear targets has also revealed a pronounced shadowing effect at small values of the Bjorken variable  $x = Q^2/2M\nu$ . Recent measurements in the kinematical range  $0.3 \text{ GeV}^2 < Q^2 < 3.2 \text{ GeV}^2$  (EMC [7]) and  $1 \text{ GeV}^2 < Q^2 < 20 \text{ GeV}^2$  (NMC [8]) show a systematic reduction of the nuclear structure functions  $F_2^A(Q^2, x)$  with respect to  $A$  times the free nucleon structure function  $F_2^N(Q^2, x)$  at  $x < 0.1$ . This observation has stimulated a great deal of theoretical activity, with attempts to describe this shadowing effect either in terms of quark-gluon dynamics on the light cone [9–11] or in complementary hadronic language [12–14].

Our aim here is to investigate the role of vector meson dominance phenomena in these processes. We point out [15] that VMD in its simplest form is by far not sufficient to understand the behaviour of the free nucleon structure function  $F_2^N$  at small  $x$ , whereas it may still be an important factor in the shadowing mechanism [15].

Let us first return to the propagation length (11) of hadronic fluctuations of the photon. We have already mentioned that  $\lambda \doteq 1/Mx = 0.21 \text{ fm}/x$  reaches nuclear dimensions

for  $x < 0.1$ . Consider now a description of deep-inelastic lepton scattering on nucleons or nuclei in the laboratory frame with the target at rest. In this frame the basic diagrams representing the interaction of the virtual photon with the nucleon involve time orderings as shown in Figs. 7a and b: the photon either hits a quark in the target which then picks up the large incident momentum and energy, or the photon converts into a quark-antiquark pair which subsequently interacts with the target. At small  $x$ , the pair production term Fig. 7b dominates. This can be seen by comparing the energy denominators of the processes illustrated in Fig. 7 in standard "old fashioned" perturbation theory. Let  $m_q$  be a typical (constituent) quark mass. For large energy transfer  $\nu \gg m_q$  and  $\nu^2 \gg Q^2$  the characteristic energy difference for process (a) is  $\Delta E_a \equiv E_a(t_2) - E_a(t_1) \sim -m_q + \frac{m_q^2 + Q^2}{2\nu}$ . In process (b), let the quarks in the produced  $q\bar{q}$ -pair carry momenta  $\vec{q}/2 + \Delta\vec{q}$  and  $\vec{q}/2 - \Delta\vec{q}$ , respectively. We assume that the relative momentum of the pair is small compared to its total momentum:  $|\Delta\vec{q}| \ll |\vec{q}| = \sqrt{Q^2 + \nu^2}$ . In fact  $|\vec{q}|$  is of order 10 GeV or larger in our kinematical range, whereas the typical hadronic scale which governs the relative motion of the  $q\bar{q}$ -pair implies  $|\Delta\vec{q}| < 1$  GeV. Therefore we find for the energy difference in process (b):  $\Delta E_b \equiv E_b(t_2) - E_b(t_1) \sim \frac{4m_q^2 + Q^2}{2\nu}$ . Consequently the ratio of magnitudes of the quasifree amplitude  $A_a$  and the pair amplitude  $A_b$  behaves roughly like

$$\left| \frac{A_a}{A_b} \right| \sim \frac{\Delta E_b}{\Delta E_a} \sim \frac{Q^2}{2m_q\nu} \left[ 1 + \frac{4m_q^2}{Q^2} \right]. \quad (15)$$

This ratio is evidently small compared to unity for  $x < 0.1$ . Hence the  $q\bar{q}$ -pair mechanism, Fig. 7b, dominates at small  $x$ . The further evolution of the process will then lead to the mechanism in which a hadronic state, carrying photon quantum numbers, strongly interacts with the nucleon.

This picture implies that in deep-inelastic scattering at small  $x$ , the virtual photon primarily interacts with a nucleon or nucleus through the scattering of its hadronic components on the target. Nuclear shadowing is expected to occur when the coherence length  $\lambda$  of the hadronic intermediate state exceeds the average distance between two nucleons in the nucleus, i.e. when double scattering starts to occur. With  $d \simeq 1.8$  fm and  $\lambda > d$  this implies  $x < 1/Md \simeq 0.1$  as a condition for shadowing.

### 5.2.1 Free Nucleon Structure Function

The free nucleon structure function  $F_2^N(Q^2, x)$  (introduced here as the average of proton and neutron structure functions) can be written

$$F_2^N(Q^2, x) = \frac{Q^2}{\pi e^2} \sigma(\gamma^* N) \quad (16)$$

in terms of the virtual photon-nucleon cross section (the sum of longitudinal and transverse cross sections). Following the previous discussions we assume that, at small  $x$ , the virtual photon interacts with the nucleon by first converting into a  $q\bar{q}$  - pair which then propagates and interacts strongly with the nucleon. This leads to the following

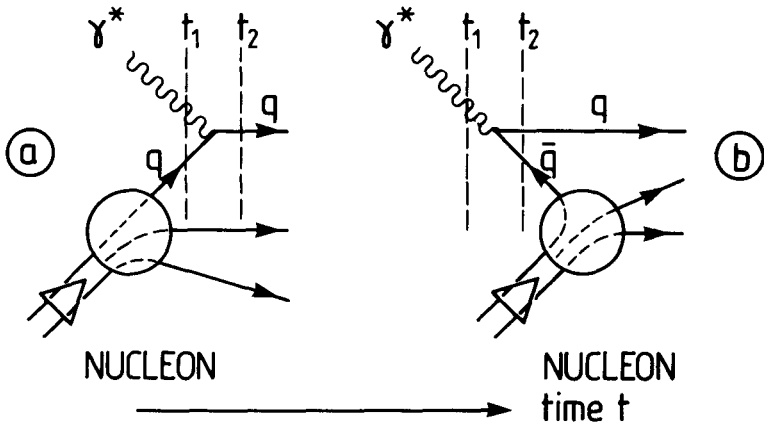


**Figure 7:** Time orderings in a lab. frame description of virtual photon–nucleon interactions. The active quark (or antiquark) is denoted by  $q$  (or  $\bar{q}$ ).

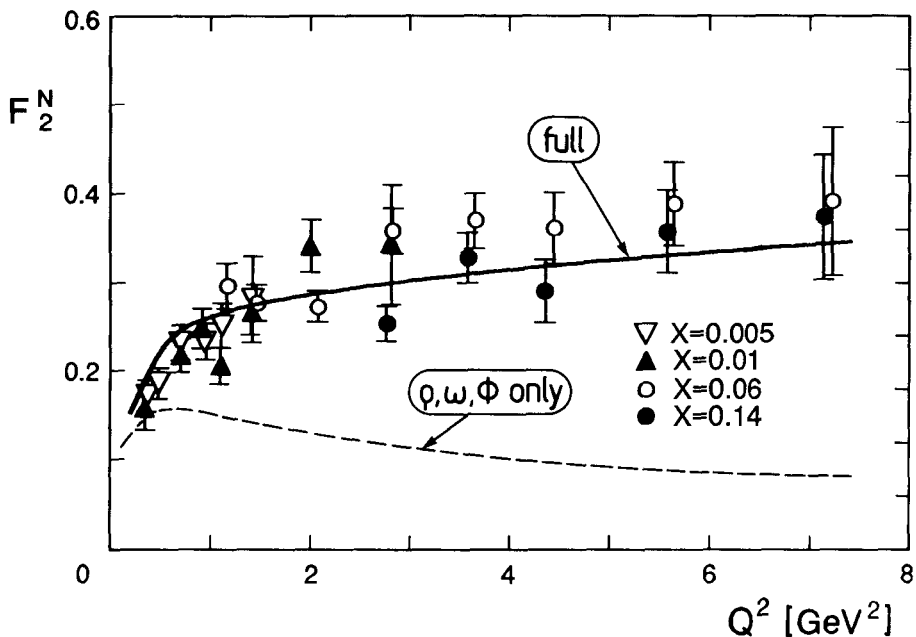


**Figure 8:** Free nucleon structure function for small values of  $x$ . Data from ref. [17]. The solid curve is obtained from eq. (17) with  $\sigma_N = 16 \text{ mb} \cdot \text{GeV}^2/\mu^2$ . The dashed line incorporates the low mass vector mesons ( $\rho, \omega, \phi$ ) only.

approximate form of the structure function, valid at small  $x$ :

$$F_2^N(Q^2, x) = \frac{Q^2}{\pi} \int_{4m_\pi^2}^{\infty} d\mu^2 \frac{\mu^2 \Pi(\mu^2)}{(\mu^2 + Q^2)^2} \sigma_N(\mu^2; s \simeq Q^2/x). \quad (17)$$

Here  $\Pi(\mu^2)$  is the mass spectrum of hadronic components of the photon, as given by eq. (9). The factor  $(\mu^2 + Q^2)^{-2}$  is the squared propagator of these fluctuations, and  $\sigma_N(\mu^2; s)$  is the effective cross section for the scattering of a hadronic state of mass  $\mu$  from the nucleon. The energy variable in  $\sigma_N$  is  $s = 2M\nu + M^2 - Q^2 \simeq Q^2/x$ .

The effective cross section  $\sigma_N$  summarizes all interactions of hadronic components of the photon with the composite nucleon. For small  $x$  the hadron-nucleon center-of mass energy  $\sqrt{s}$  is in the multi-GeV range where cross sections are flat. We therefore use an average  $\sigma_N$ , independent of  $s$ . The leading dependence of  $\sigma_N$  on the hadron mass  $\mu$  should satisfy the following criteria:

- i) For large  $Q^2$ , the structure function  $F_2^N$  should have the proper scaling behaviour, i.e. it should become independent of  $Q^2$ . This requirement is fulfilled with the ansatz  $\sigma_N = \text{const.}/\mu^2$ . By inspection of the integral (17) it is indeed obvious that such a  $\mu^{-2}$  dependence of  $\sigma_N$  leads to scaling.
- ii) Empirical vector meson-nucleon cross sections follow roughly a  $1/\mu^2$  rule.

We see this from table 1 where the ansatz

$$\sigma_N(\mu^2) = \frac{16mb \cdot GeV^2}{\mu^2} \quad (18)$$

is compared with the available vector meson cross sections deduced from photoproduction data.

	$\sigma_{VN} [\text{mb}]$	
	empirical	from eq. (18)
$\rho$	$27 \pm 3$	26
$\omega$		
$\phi$	$12 \pm 3$	15
$J/\Psi$	$2 \pm 1$	2

Table 1: Vector meson-nucleon cross sections: empirical values [6, 16] (left) compared with the ansatz, eq. (18)

The simple ansatz (18), together with the empirical  $\Pi(\mu^2)$  from  $\sigma(e^+e^- \rightarrow \text{hadrons})$  according to eq. (9), reproduces the nucleon structure function at small  $x$  remarkably well. This is demonstrated in Fig. 8. Note that the ansatz (18) makes  $F_2^N$  independent of  $x$  for small  $x$ . This is consistent with the data [17] within (admittedly sizeable) error bars. At the same time Fig. 8 clearly shows that the standard vector meson dominance model is unable to reproduce the  $Q^2$  dependence of  $F_2^N$ . When the spectrum  $\Pi(\mu^2)$  is cut off at  $\mu^2 = m_\phi^2 \sim 1 \text{ GeV}^2$  so that only the low-mass vector mesons contribute, a major part of the strength in  $F_2^N$  is obviously missing for  $Q^2 > 1 \text{ GeV}^2$ : the  $q\bar{q}$ -continuum with masses  $\mu > 1 \text{ GeV}$  is very important to reproduce  $F_2^N$  at small  $x$ .

We note that in principle,  $F_2^N$  of eq. (17) could have been written in the more general form of a double dispersion relation [18] in order to account for off-diagonal diffractive dissociation processes (such as  $VN \rightarrow V'N$  where  $V$  and  $V'$  are two different vector meson states). However, the authors of ref. [13] have pointed out strong destructive interferences between such on- and off-diagonal terms. Remaining effects are then thought to be absorbed in the parametrization of the effective cross section  $\sigma_N(\mu^2)$ .

### 5.2.2 Nuclear Structure Function

Next we describe the nuclear structure function  $F_2^A$  at small  $x$  using exactly the same model as previously developed. We write

$$F_2^A(Q^2, x) = \frac{Q^2}{\pi} \int_{4m_\pi^2}^{\infty} d\mu^2 \frac{\mu^2 \Pi(\mu^2)}{(\mu^2 + Q^2)^2} \sigma_A(\mu^2; s), \quad (19)$$

where  $\sigma_A$  is now the effective hadron-nucleus cross section. Given the large photon energy  $\nu$  it is justified to use the eikonal approximation and employ Glauber multiple scattering theory to connect  $\sigma_A$  and  $\sigma_N$ .

A typical feature at high energy is the smallness of  $\text{Re } f_N/\text{Im } f_N$ , the ratio of real and imaginary parts of the forward hadron-nucleon amplitudes; we assume this ratio to be negligible. We also neglect diffractive dissociation terms  $VN \rightarrow V'N$  in the multiple scattering series. This could lead to an error of about 5 % in  $\sigma_A$  due to inelastic screening effects [19].

An important point is that the propagation length  $\lambda$  of intermediate hadronic states has to be taken into account properly. This is done by an extension of Glauber theory as described by Gribov [20]. The finite coherence length  $\lambda = 2\nu/(Q^2 + \mu^2)$  enters in a characteristic phase factor. It first appears in the double scattering term as  $\exp[i(z_1 - z_2)/\lambda]$  and has an obvious interpretation: if  $\lambda$  is large compared to the distance  $d = z_1 - z_2$  between two nucleons in the target, the phase factor is close to unity and double scattering occurs with full strength. However, if  $\lambda \ll d$ , then this phase factor rapidly oscillates and double scattering is suppressed.

Altogether we end up with the following expression:

$$\sigma_A(\mu^2; s) = A\sigma_N(\mu^2; s) + \\ + \sum_{n=2}^A \left( -\frac{1}{2} \right)^{n-1} \binom{A}{n} \left[ \frac{\sigma_N(\mu^2; s)}{A} \right]^n Re \left\{ \int d^2 b dz_1 ... dz_n \rho_n(\vec{b}, z_1, ..., z_n) e^{i(z_1 - z_n)/\lambda} \right\}. \quad (20)$$

Here  $\rho_n$  is the n-particle nuclear density with coordinates taken along the path of the scattering hadron, i.e. parallel to the z-axis at an impact parameter  $\vec{b}$ . We expand  $\rho_n$  up to terms linear in the two-body correlation function  $\Delta(\vec{r}, \vec{r}') = \rho_2(\vec{r}, \vec{r}') - \rho(\vec{r})\rho(\vec{r}') \equiv g(\vec{r}, \vec{r}')\rho(\vec{r})\rho(\vec{r}')$  where  $\rho(\vec{r})$  is the one-body density:

$$\rho_n(\vec{b}, z_1, ..., z_n) = \rho(\vec{b}, z_1) ... \rho(\vec{b}, z_n) + \sum_{\text{all permutations}} \Delta(\vec{b}, z_1, z_2) \rho(\vec{b}, z_3) ... \rho(\vec{b}, z_n). \quad (21)$$

In practice we use for the correlation factor  $g(|\vec{r} - \vec{r}'|)$  a simple parametrization which approximates the nuclear G-matrix [21]. We also use realistic nuclear density distributions  $\rho(r)$  which fit elastic electron scattering data.

With these ingredients we have calculated [15] the ratio

$$R(Q^2, x) = \frac{F_2^A(Q^2, x)}{A F_2^N(Q^2, x)} \quad (22)$$

of the nuclear and free nucleon structure functions for  $x < 0.1$  and compare with recent data for  $^{12}\text{C}$  and  $^{40}\text{Ca}$  as obtained by the NMC collaboration at CERN. These data at small  $x$  cover the range  $1 \text{ GeV}^2 < Q^2 < 20 \text{ GeV}^2$  with a 200 GeV incident muon beam energy. Results are shown in Fig. 9. We find that the pronounced shadowing observed at  $x < 0.1$  can in fact be reproduced quite well in our simple model. Note that in this calculation, no additional free parameters have been introduced beyond the effective cross section  $\sigma_N = 16mb \cdot \text{GeV}^2/\mu^2$  which enters in  $F_2^N$  for the free nucleon. The shadowing effect turns out to be dominated (see Fig. 9) by the low-mass vector meson components of the spectrum  $\Pi(\mu^2)$ ; their propagation length  $\lambda$  is large compared to the nuclear size. Components of large mass  $\mu$ , even though they are very important in the free structure function  $F_2^N$ , are much less effective in the shadowing process since their propagation length is shorter; in addition the  $1/\mu^2$  behaviour of the effective cross section  $\sigma_N$  suppresses multiple scattering for large  $\mu$ .

Much discussion has recently been devoted to the  $Q^2$  dependence of the shadowing effect [10, 14]. We show in Fig. 10 a comparison of our calculations with the earlier EMC data [7] which involve lower  $Q^2$  values ( $0.3 \text{ GeV}^2 < Q^2 < 3.2 \text{ GeV}^2$ ) than the new NMC data. We do this also in order to show the smooth  $Q^2$  dependence of our model, which turns out to be close to a logarithmic one for  $1 \text{ GeV}^2 < Q^2 < 10 \text{ GeV}^2$ . For  $Q^2$  much larger than  $10 \text{ GeV}^2$ , the shadowing effect disappears, as one would expect.

At  $Q^2 = 0$ , the present model reproduces quite well the nuclear shadowing observed with real photons at  $\nu = 50 - 100 \text{ GeV}$  (see section 5.1 and ref. [22]): we find  $\sigma_{\gamma A} = A^{0.91} \sigma_{\gamma N}$  in this energy range.

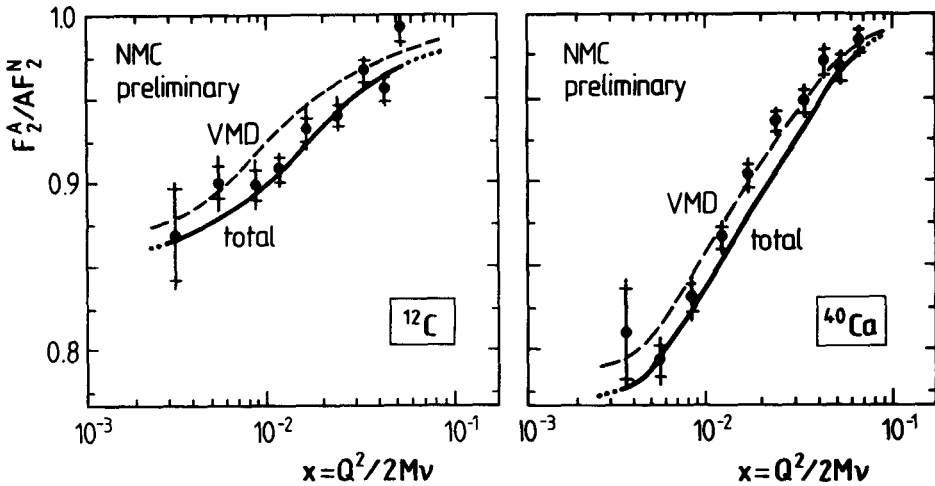


**Figure 9:** Ratio of nuclear and free nucleon strucure function at small  $x$  for  $^{12}C$  and  $^{40}Ca$ . Preliminary data of the NMC collaboration [8]. The solid curve is calculated using eqs. (19, 20). The dashed curves are obtained by including only the  $\rho$ ,  $\omega$  and  $\phi$  mesons in the mass spectrum  $\Pi(\mu^2)$ .

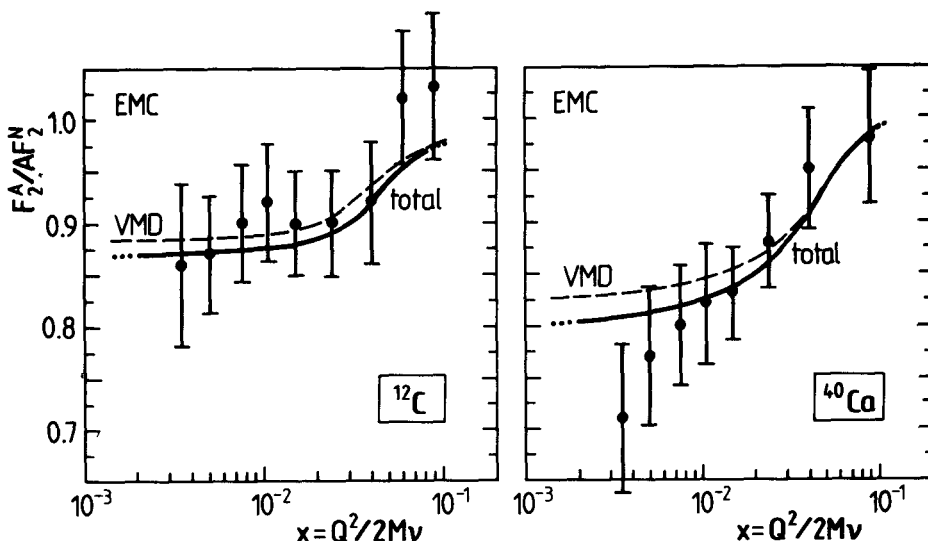


**Figure 10:** Same as Fig. 9, but for the EMC data [7].

## 6. SUMMARY

Vector mesons play an important role in the electromagnetic interactions of hadrons. They govern hadron form factors at  $q^2 < 1 \text{ GeV}^2$ ; they are responsible for a large part of the pronounced hadronic shadowing effects seen with real photons in the multi-GeV range. One of our primary aims in this presentation was to explore to what extent vector meson dominance still plays a role in deep-inelastic scattering at small  $x$  where sea-quarks become important. This question has been subject of some debate [10, 14]. We find that the free nucleon structure function at small  $x$  can not at all be reproduced by the "naive" version of VMD, with only  $\rho$ ,  $\omega$  and  $\phi$  included. It is of crucial importance to incorporate the higher mass quark-antiquark continuum in the description. On the other hand, the shadowing phenomenon in the nuclear structure function at  $x < 0.1$  is still governed by the low-mass vector meson states, at least in our simple model. It is of interest to explore the possible connections between the phenomenological hadronic description presented here and the QCD-based approaches of refs. [9–11].

We would like to thank Gerry Brown, John Durso, Jerry Miller, Kazuo Takayanagi and Mark Strikman for illuminating discussions. One of us (W.W.) enjoyed the kind hospitality of the Theory Group at GSI (Darmstadt) during the preparation of these notes.

## References

1. M. Gell-Mann and F. Zachariasen, Phys. Rev. **124** (1961) 953;  
J.J. Sakurai, Currents and Mesons, Univ. of Chicago Press (1969)
2. J. W. Durso, Phys. Lett. B **184** (1987) 348
3. S. R. Amendolia et al., Nucl. Phys. B **277** (1986) 168
4. J. Ahrens, Nucl. Phys. A **446** (1985) 229; and refs. therein
5. G. Grammar and J. D. Sullivan, in: Electromagnetic Interactions of Hadrons, Vol. 2, A. Donnachie and G. Shaw, eds., Plenum, NY (1978), p. 195;  
W. Weise, Phys. Reports **22** (1974) 53
6. T. H. Bauer, R. D. Spital, D. R. Yennie and F. M. Lipkin, Rev. Mod. Phys. **50** (1978) 261
7. M. Arneodo et al. (EMC Collaboration), Phys. Lett. B **211** (1988) 493
8. NMC preliminary data (E. M. Kabuss, these proceedings)
9. E. L. Berger and J. Qiu, ANL-HEP-CP-88-42;  
J. Qiu, Nucl. Phys. B **291** (1987) 746;  
A. H. Mueller and J. Qiu, Nucl. Phys. B **268** (1986) 427
10. J. D. Bjorken, in: Particles and Detectors: Festschrift for Jack Steinberger, K. Kleinknecht and T. D. Lee, eds., Springer Tracts in Mod. Phys. **108** (1986) 17
11. F. E. Close, J. Qiu and R. G. Roberts, Phys. Rev. D **40** (1989) 2820;  
F. E. Close and R. G. Roberts, Phys. Lett. B **213** (1988) 91
12. G. Shaw, Phys. Lett. B **228** (1989) 125;  
P. Ditsas and G. Shaw, Nucl. Phys. B **113** (1976) 246;  
D. Schildknecht, Nucl. Phys. B **66** (1973) 398
13. C. L. Bilchak, D. Schildknecht and J. D. Stroughair, Phys. Lett. B **214** (1988) 441
14. L. Frankfurt and M. Strikman, Nucl. Phys. B **316** (1989) 340;  
S. J. Brodsky and H. J. Lu, Phys. Rev. Lett. **64** (1990) 1342;  
J. Kwiecinski and B. Badelek, Phys. Lett. B **208** (1988) 508
15. G. Piller and W. Weise, Univ. Regensburg preprint TPR-90-38 (1990)
16. J. J. Aubert et al., Nucl. Phys. B **213** (1983) 1
17. M. Arneodo et al. (EMC collaboration), Nucl. Phys. B **333** (1990) 1
18. H. Fraas, B. J. Read and D. Schildknecht, Nucl. Phys. B **86** (1975) 346
19. P. V. R. Murthy et al., Nucl. Phys. B **92** (1975) 269
20. V. N. Gribov, Sov. Phys. JETP **30** (1970) 709
21. G. E. Brown, S. O. Bäckman, E. Oset and W. Weise, Nucl. Phys. A **286** (1977) 191
22. D. O. Caldwell et al., Phys. Rev. Lett. **42** (1979) 553